An Experimental Investigation concerning the Effects of AFP Defects on Progressive Failure of Tensile Coupons

Rafal Anay[1], Paul Ziehl[8], Addis Tessema[2], Roudy Wehbe[3], Lateef Assi[4],
Addis Kidane[5], Ramy Harik[6], Brian F. Tatting[7], Zafer Gürdal[8]
University of South Carolina, Columbia, SC 29201, USA

I. Abstract

This paper discusses characterization approaches for the evaluation of potential defects that may occur during the automated fiber placement (AFP) process. Two nondestructive evaluation techniques were utilized simultaneously, acoustic emission (AE) and digital image correlation (DIC), to investigate correlations between mechanical properties and damage propagation during tension tests. The layup configuration is designed with the defect running across the width, and the stacking sequence with seven layers is produced: $[-45/0/45/\overline{90}]_s$. A total of 3 panels were manufactured: one containing a gap defect in the middle layer, another one with an overlap defect, and a pristine panel for baseline comparison. Each panel accommodates six coupons having dimensions of 20" x 2". The results indicate that defects caused during the manufacturing process affect damage initiation and growth.

II. Introduction

Automated fiber placement (AFP) is an advanced method of manufacturing composite materials. These materials are increasingly used in airframes and other industrial products. The main goal of using AFP machines is to increase the rate and precision in the production of advanced composite parts. During this manufacturing process, plies are laminated in a predesigned order and cured through an autoclave or infusion process [1]. This procedure is sensitive and micro-defects cannot always be avoided. Many types of manufacturing-induced defects may occur including resin-rich areas, voids, distorted fibers, broken/missing fibers, fiber misalignment, stacking sequence disorder, and inclusions [2-5]. These defects may increase the degradation rate of composite components and may cause failure at an earlier stage than expected. Gaps and overlaps between tows that can result from either misalignment of the tows or by design considerations in steered fiber tows were chosen for this study. To investigate correlations between mechanical properties and damage propagation, two nondestructive evaluation techniques were utilized simultaneously, acoustic emission (AE) and digital image correlation (DIC). AE is an elastic wave generated by microstructural damage, and commonly detected by piezoelectrical sensors. At least 3 AE sensors are required to determine the damage source location in two dimensions. AE signals have been used to detect and classify damage in composite materials into different mechanisms including: a) matrix cracking, b) interfacial debonding, c) fiber-matrix friction/fiber pull out, and d) fiber breakage [6, 7]. Digital image correlation is a non-contact technique utilizing a random speckle pattern, often on the surface of the specimen. Through this approach a two-dimensional strain field can be inferred.

The paper presents the experimental results introduced here for several defect-induced specimens. An accompanying paper will detail the numerical modeling of the responses and provide comparisons to these experimental results.

[1] Ph.D. Candidate, Department of Civil and Environmental Engineering
[2] Ph.D. Candidate, Department of Mechanical Engineering
[3] Ph.D. Candidate, Department of Mechanical Engineering
[4] Ph.D. Candidate, Department of Civil and Environmental Engineering
[5] Associate Professor, College of Engineering and Computing
[6] Associate Professor, College of Engineering and Computing
[7] Research Assistant Professor, College of Engineering and Computing – McNAIR Center
[8] Professor, College of Engineering and Computing

III. Specimen Configuration and Manufacture

The purpose of the specimen design with embedded defects is to replicate defects that may occur during AFP manufacturing. For this reason, only one defect layer is placed in the middle of the specimen since the occurrence of these defects simultaneously at the same location is very rare. In addition, a symmetric and balanced near quasi-isotropic layup is used to minimize coupling terms in the ABD matrix (classical lamination theory). The layup configuration is designed with the defect running across the width. Based on this condition, the stacking sequence with seven layers is produced: $[-45/0/45/\overline{90}]_s$. The overbar in the representation defines a single layer at the laminate mid-plane. A total of 3 panels were manufactured: one containing a gap defect in the middle layer, another one with an overlap defect, and a pristine panel for baseline comparison (Fig. 1). Each panel accommodates six coupons having dimensions of 20" x 2". Relatively large size coupons are necessary to obtain better accuracy for acoustic emission source location. The size of both defects placed in the middle of the specimen is determined to be half a tow width ($1/8^{th}$ of an inch) since a larger defect size during AFP is unusual. For the manufacturing of the defective panels, the middle layer is divided into several regions where these regions are either overlapping by $1/8^{th}$ of an inch or spaced apart by the same distance depending on the layup configuration. Therefore, the AFP machine is automatically programmed to produce these defects without human intervention during the manufacturing process. The AFP Lynx machine at the McNAIR center is used to manufacture the panels using ¼ inch tows, Hexcel IM7-8552 material [8]. The produced panels are cured with caul plates in the autoclave using the curing cycle recommended by the manufacturer [8]. A water jet is used to cut the coupons from the produced panels. The cutting profile for the coupons is programmed so that the defect is located at the center across the width coupon.

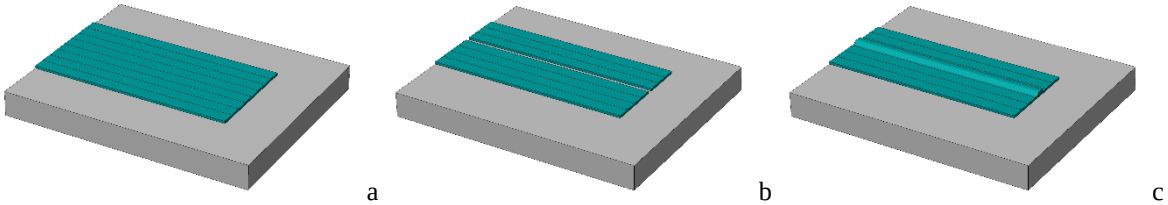

a b c

Fig. 1 Layup configuration, a: pristine, b: gap between tows, c: overlap between tows.

IV. Experimental Setup

Both digital image correlation and acoustic emission techniques were utilized for assessing damage during tensile loading of pristine and defect-induced specimens. Acoustic emission sensors were affixed to one side of each specimen while digital image correlation was used on the opposite side to prevent interference from the sensor attachments with the speckle pattern. The following addresses experimental details of the two methods.

A. Digital Image Correlation (DIC)

2D digital image correlation (2D DIC) is used in-situ to capture the deformation. An area of interest is chosen at the center of the gage length and a random black speckle pattern is made over white plain background using flat spray paint as shown in Fig.2. The DIC system consists of a 5 MPixel camera coupled with 60 mm lens and LED powered lamp, as shown in Fig. 4. Images of the speckled region were acquired at a rate of 1 frame per second. The images are then post-processed using commercial software VIC-2D (Correlated Solution Inc.) to obtain the deformation/strain of the coupon.

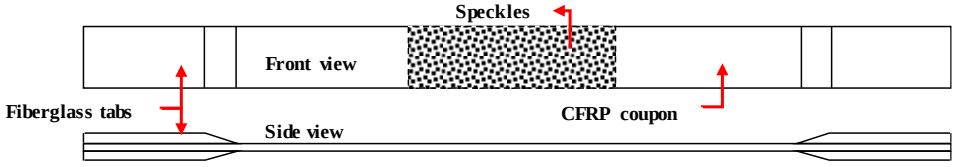

Fig. 2 Test coupon with Fiberglass tabs and surface speckles

B. Acoustic Emissions (AE)

Six AE broadband sensors, type B-1025 (Digital Wave Corporation, Castle Rock, Colorado), were used having an operating frequency range between 50-2000 kHz. Hot melt glue was utilized as a coupling agent to fix the sensors on one surface of the specimens. AE signal preamplifiers (type 2/4/6, MISTRAS Group Inc., Princeton Junction, New Jersey) supplied 40 dB gain and band pass filters from 100 to 1200 kHz were used. The digital AE data acquisition system was a 24-channel Micro II Express (Mistras Group Inc.). The AE sensor layout and photographs of the test setup are shown in Figs. 3 and 4. Prior to conducting loading of the specimens, a background noise check was performed to identify the appropriate testing threshold (31 dB). Pencil lead breaks (PLB) were utilized prior to loading to assess the sensitivity of each sensor and to ensure that the coupling was consistent for all sensors.

Tension tests were conducted using a Material Testing System (MTS 810) with a servo-controlled hydraulic loading frame. The specimens were loaded in displacement control at a rate of 0.02 in/min. The first specimen of each type was loaded to failure without attaching AE sensors to determine the ultimate capacity. The results served as a guide for the next part of the test; hence, subsequent specimens were loaded to 80% of the ultimate load. Once 80% of the ultimate load was reached, AE sensors were removed and the specimens was loaded to failure.

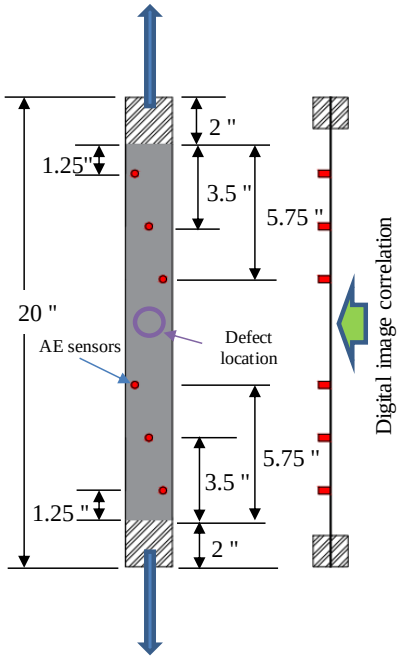

Fig. 3 AE sensor layout

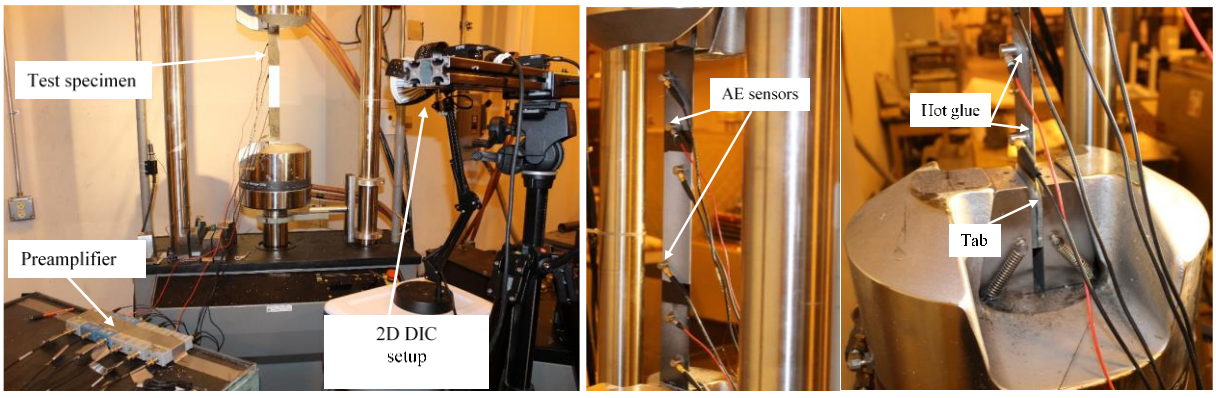

Fig. 4 Photographs of test setup

V. Experimental Results

The ultimate capacity (average of 6 specimens) of each layup is shown in Fig. 5. As expected, specimens with an overlap defect show superiority in strength over the pristine and full gap specimens. The pristine specimens have relatively higher strength than the full gap defect specimen. It should be noted that the overlap samples have extra fibers in the laminate, while the specimen with gap defect has less fibers compared to the pristine samples. Thus, such variation in failure load is related to fiber counts within the different groups of specimens.

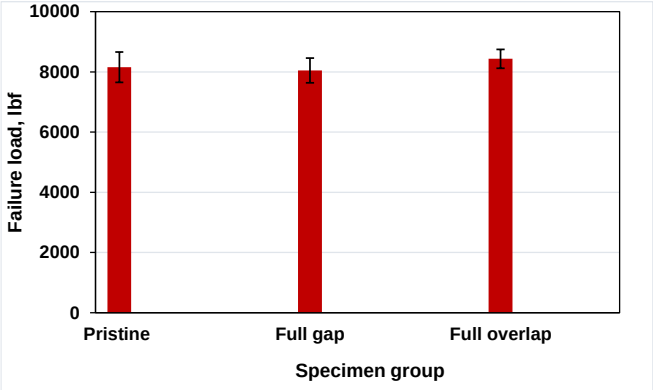

Fig. 5 Failure load for the different group of laminates

Detection and Assessment of Active Damage Progression

Acoustic emission data was recorded and post-processed with AEwin software [9]. AE data initiated early in the test (approximately 10% of ultimate) and continued thereafter. Cumulative signal strength (CSS) as a function of load is shown in Fig. 6. Significant jumps in CSS compared with the previous stages were observed and used to distinguish between the divided regions. In each region, several ranges of damage progression, illuminated by changes in the slope of the cumulative signal strength curve, can be observed. In the first region (R1, from zero to about 40% of the ultimate load), higher damage was seen in the gap specimen than the overlap and pristine specimens. After that, clear differences in CSS among the specimens were seen in region 2 (from 40% to 80% of ultimate load) which indicates more damage accumulation in the gap specimen than the other specimens.

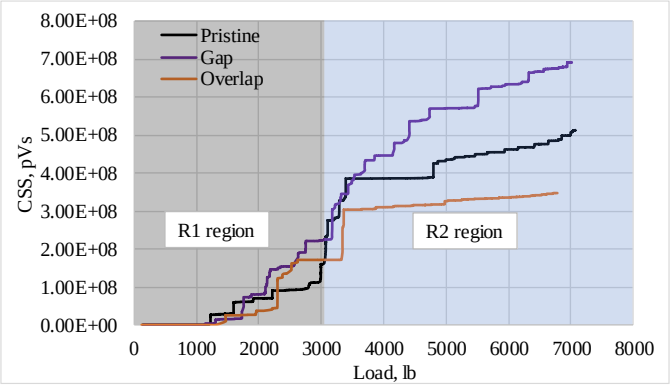

Fig. 6 Cumulative signal strength versus load

Source Localization of Acoustic Emission Events

Source localization algorithms based on time of flight were utilized (AEWin, [9]). The wave speed was determined through 0.3 mm diameter 2H pencil lead break tests. The proper identification of wave reflections from cracks and structural boundaries is an important issue in source localization. Source location of unfiltered data was first conducted to determine if the results were reasonable and if filtering of the data was required. Figs. 7 and 8 show 2D maps of AE events collected during tensile loading of pristine and gap specimens. The test was divided into five stages as a percentage of ultimate load and one 2D map was generated for each stage. As seen in Fig. 7, only a few events were detected up to 36% of ultimate load which were located near the bottom end. It is believed that these events are due to the end condition. Then, new events were detected and localized from 53% of ultimate load to the end of the test in the 45^{o} and 90^{o} layers represented by yellow and green events respectively. The results shown in Fig. 7 approximately correspond to the failure pattern of the pristine specimen. Similar behavior was observed in the 2D maps of the gap specimen (Fig. 8) except that more events were located near the mid region of the specimen (between sensors 3 and 4) considered to be due to induced defect (missing tow in the 90^{o} layer).

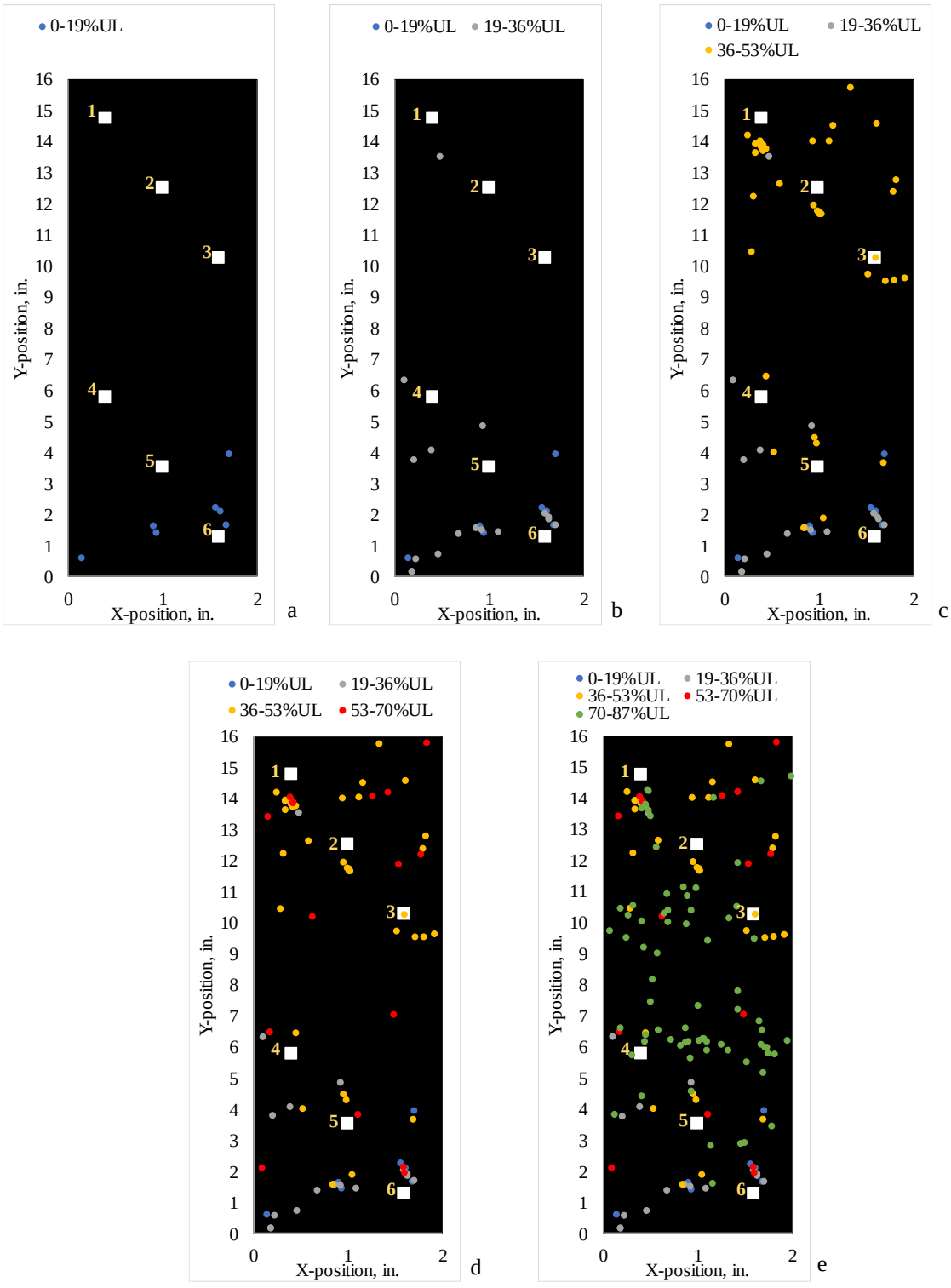

Fig. 7 Source localization (pristine specimen)

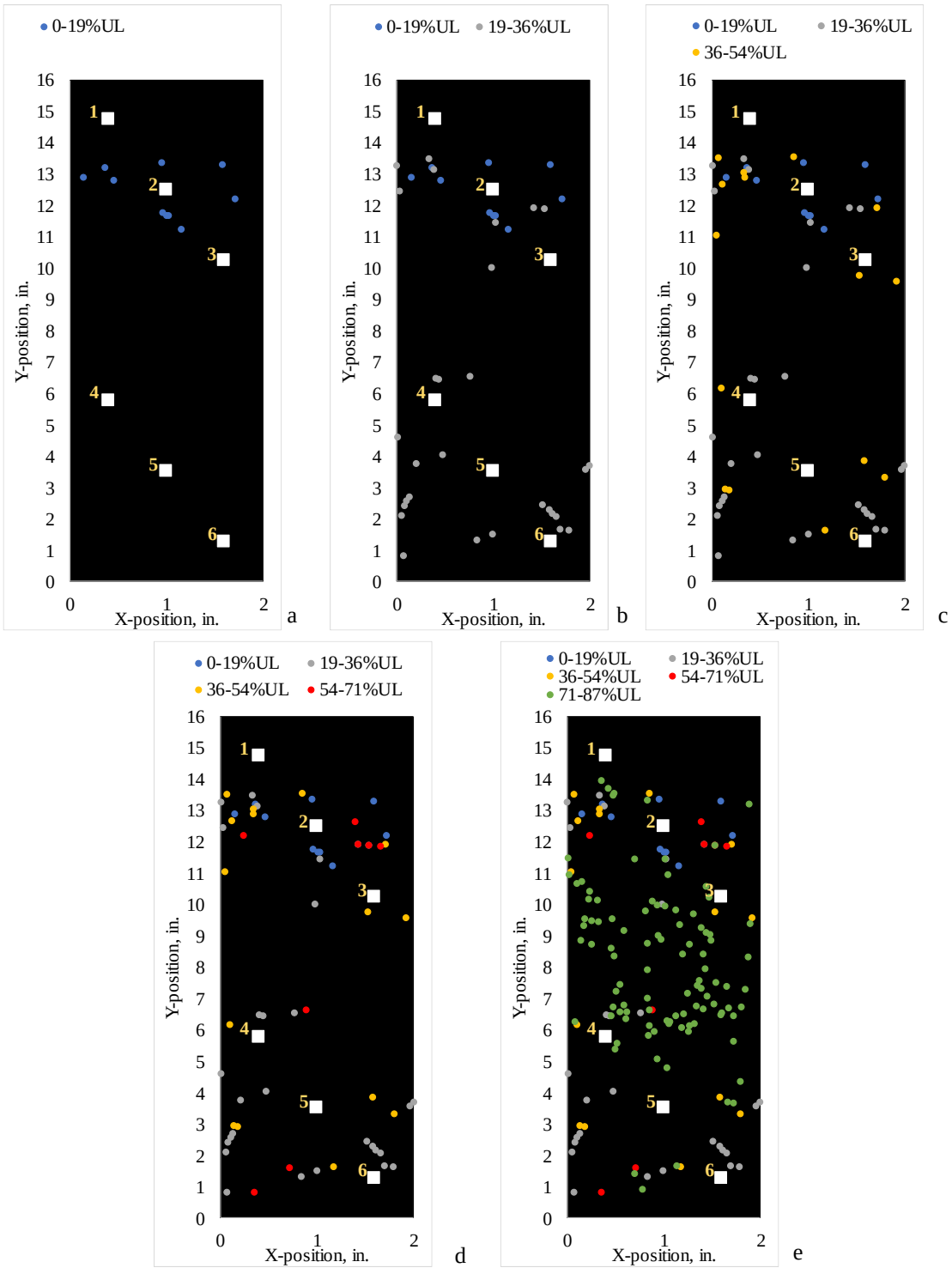

Fig. 8 Source localization (gap specimen)

DIC results

The full-field axial and transverse strain contours obtained from DIC are depicted in Fig. 9. From the axial strain contour, uniform surface strain is observed for most of the loading duration and strain localizations were observed near the final failure of the coupon as shown in Fig. 9(a). On the other hand, strain localization is started at

the early stage of loading for the transverse strain contour plot (seen in Fig. 9(b)). These strain localizations are presumed to have association with the internal cracks formed within the laminate.

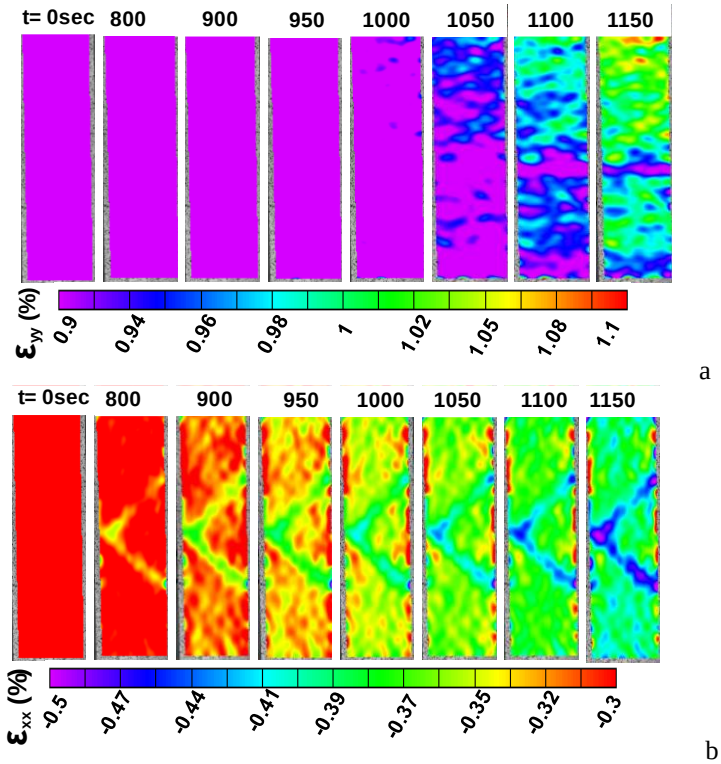

Fig. 9 Full-field strain plots (a) axial strain, ε_{yy}, and (b) transverse strain, ε_{xx}

VI. Conclusions

The results of the acoustic emission evaluation indicate the potential for assigning damage mechanisms due to tensile loading of the pristine and defect induced specimens. Cumulative signal strength was a useful parameter for understanding damage initiation and progression. Two different regions were defined depending on changes in slope of the cumulative signal strength curves. In each region, several ranges of damage progression, illuminated by several jumps in the cumulative signal strength curve were observed. Source localization gave indications of crack growth and two-dimensional maps were generated through DIC and used to investigate the different damage levels of each specimen.

Acknowledgements

This material is based upon work supported by the National Aeronautics and Space Administration (NASA) under the Advanced Composite Consortium (ACC). Any opinions, findings, and conclusions expressed in this material are those of the author(s) and do not necessarily reflect the views of NASA.

Additional support received from the McNAIR Center for specimen manufacture is gratefully acknowledged.

References

[1] Ning, W., "Structural health condition monitoring of carbon-fibre based composite materials using acoustic emission techniques," (Doctoral dissertation, University of Birmingham), 2015.
[2] Gurit, "Guide to Composites," http://www.gurit.com/guide-to-composites.aspx

[3] Bader, S., “Crystic composites handbook,” Wollaston: Scott Bader Company, 45, 2005.
[4] Cantwell, W. J., and Morton, J., “The impact resistance of composite materials—a review,” composites, *22*(5), 1991, 347-362.
[5] Hull, D., “An introduction to composite materials,” Cambridge, University Press, 1987.
[6] Chandarana, N., Sanchez, D. M., Soutis, C., & Gresil, M., “Early Damage Detection in Composites during Fabrication and Mechanical Testing,” Materials, 10(7),2017, 685.
[7] Godin, N., Huguet, S., & Gaertner, R., “Integration of the Kohonen's self-organising map and k-means algorithm for the segmentation of the AE data collected during tensile tests on cross-ply composites,” NDT & E International, 38(4), 2005, 299-309.
[8] HexPly® 8552, Product Data Sheet, URL: http://www.hexcel.com/user_area/content_media/raw/HexPly_8552_us_DataSheet.pdf
[9] AEwin software version e4.30, Mistras Group Inc. http://www.physicalacoustics.com/by-product/aewin/, 2010.